DOI: 10.1002/((please add manuscript number))
Article type: Communication

Solution-Processed Neodymium Oxide/ZnO Thin Film Transistors with Electron Mobility in Excess of 65 cm^2 /Vs

Mazran Esro, Oleg Kolosov, Vlad Stolojan, Peter J. Jones, William I. Milne and *George Adamopoulos**

Dr. G. Adamopoulos*, M. Esro, P. J. Jones
Lancaster University,
Engineering Department
Lancaster LA1 4YR, UK
E-mail: g.adamopoulos@lancaster.ac.uk

Prof. O. Kolosov
Quantum Technology Centre
Department of Physics
University of Lancaster
LA1 4YW, UK

Dr. V. Stolojan
Advanced Technology Institute
Electronic and Electrical Engineering
University of Surrey
Guildford, GU2 7HX, U.K

Prof. W. I. Milne
Department of Engineering
University of Cambridge
9 JJ Thomson Avenue
Cambridge CB3 0FA, UK

And

Quantum Nanoelectronics Research Center (QNERC)
Tokyo Institute of Technology
2-12-1 Ookayama, Meguro-ku
Tokyo, 152-8550, JAPAN

Keywords: Gate dielectrics, neodymium oxide, solution processed electronics, spray pyrolysis, thin film transistors

A wide range of rare-earth metal oxides (REOs) constitute promising candidates for high-*k* gate dielectrics, as they combine excellent dielectric properties i.e. high dielectric constant and low

leakage currents with wide band gaps, in the range between 3.9 and 6 eV. [1-7][1],[2],[3],[4],[5],[6],[7] Yet, another attractive feature of rare-earth oxides that further boosted their research is the excellent stability and interface properties with silicon.[4,8-9] Also, their relatively close lattice constant match to silicon further enhances the possibility of epitaxial growth. Epitaxial growth of REOs (i.e. Gd_2O_3) on GaAs has also been reported,[10,11] and further investigations[12,13] demonstrated their potential applications in a number of III-Vs-based optoelectronic devices.

Despite their relatively short history, metal oxide semiconductor-based thin film transistors (TFTs) constitute a promising technology for application in large-area electronics and have already been produced with high electron mobility, excellent chemical stability, mechanical stress tolerance and high optical transparency.[14-23]

Due to their wide band gaps (>3 eV) however, metal oxide-based semiconductors require gate dielectrics with a relatively wide band gap (potential barrier at each band greater than 1 eV) in order to inhibit conduction by the Schottky emission of electrons or holes into the oxide bands.[3,24] A number of wide band gap REOs (La_2O_3, Y_2O_3, Nd_2O_3) have shown promise for implementation in TFTs employing metal oxide semiconducting channels.

Among those, neodymium oxide (Nd_2O_3) has been investigated and films with different crystal structures and properties have been successfully produced. However their successful implementation in operating TFTs has been rather limited.[25]

Depending on the deposition technique and substrate temperature, Nd_2O_3 can adopt either an amorphous (a-Nd_2O_3), cubic (c-Nd_2O_3) or hexagonal (h-Nd_2O_3) phase resulting in dielectric constants of about 11, 14 and 21 for the different phases respectively.[26] Regarding the latter, the dielectric constant of h-Nd_2O_3 is still under debate as contradictory results have been reported.[26-28]

Nd_2O_3 dielectrics can be deposited using a wide range of vacuum based techniques such as reactive rf sputtering,[29,30] pulsed laser deposition (PLD),[28,31] electron beam evaporation,[32] thermal evaporation,[26,33-34] inductively coupled radio frequency thermal plasma,[35] Molecular

Beam Epitaxy (MBE),[36] atomic layer deposition (ALD),[37-43] and Metal-Organic Chemical Vapor Deposition (MOCVD).[5, 44-48]

They do exhibit excellent performance but Nd_2O_3 deposition using vacuum-based techniques still requires a high substrate temperature or high temperature post-deposition annealing, which is incompatible with the use of glass substrates. A recent report however demonstrated the deposition of a range of rare earth oxides by ALD at substrate temperatures as low as 225 °C,[37] lowering even further the processing temperature by the utilization of novel precursor materials. Also, such deposition techniques still suffer from high manufacturing costs and in some instances, limited large-area deposition capabilities. To overcome this issue, significant research has been focused on the development of alternative deposition techniques based on solutions, including sol-gel,[49-51] spray pyrolysis[52,53] and dip coating.[54]

Even though the application of the above mentioned techniques successfully demonstrated the deposition of Nd_2O_3 films or nanoparticles, as indicated above, films had to undergo post-deposition annealing at high temperatures (occasionally up to ≈1200 °C), and still showed relatively low dielectric constants and poor adhesion to the substrate. Moreover, Nd_2O_3 films that were deposited (or annealed) at moderate temperatures (≈500 °C) from β-diketonate precursors had carbon contamination. The relatively small number of reports of the deposition of Nd_2O_3 by vacuum deposition techniques (MOCVD in particular) is mainly due to a lack of precursors with the appropriate volatility and decomposition characteristics. Moreover, the use of high substrate temperatures (exceeding 600 °C) is a limiting factor that rules out the use of glass (flexible glass in particular), narrowing down the substrate material of choice to those with high melting point. Additionally, the use of high substrate temperatures favors the Leidenfrost effect, resulting in low deposition rates and high film surface roughness.

We have recently demonstrated that the application of spray coating (or spray pyrolysis) at moderate temperatures - a rather simple and large-area-compatible deposition technique - can

be used for the deposition of high-quality high-*k* dielectrics based on HfO_2,[55] ZrO_2,[56] Al_2O_3/TiO_2[57] as well as REOs i.e. Y_2O_3,[58] La_2O_3 and $LaAlO_3$.[59]

In this report we further demonstrate the spray coating deposition of Nd_2O_3 gate dielectrics at moderate temperatures (≈400 ºC) over large area, in air, by using a rather common β-diketonate precursor and a combination of solvents that allow the precursor's solubility and growth rate to be optimized. The Nd_2O_3 dielectrics were deposited onto Indium Tin Oxide (ITO) coated glass (≈0.6 mm), c-Si, fused silica and KBr substrates from neodymium(III) 2,4-pentanedionate solutions in methanol, pentane-2,4-dione, N,N-Dimethyloformamide (7:2:1), as described in the experimental section. The present combination of precursor materials and solvents yielded films of excellent uniformity, with thickness standard deviation less than 1.7% over an area of 20 cm x 20 cm. We also found that for deposition at substrate temperatures below 380 ºC, films with considerably lower dielectric constant (compared to that of films deposited at temperatures in the range between 400 ºC and 550 ºC) and unacceptable high leakage currents were produced. Further increase of the deposition temperature up to 550 ºC showed some slight improvement of the optical and dielectric properties of the Nd_2O_3 dielectric layer.

The film properties were investigated using a wide range of characterization techniques including spectroscopic ellipsometry, UV–Vis absorption spectroscopy, impedance spectroscopy, x-ray photoelectron spectroscopy (XPS), atomic/ultrasonic force microscopy (AFM/UFM) and Transmission Electron Spectroscopy (TEM). The TFT characteristics were obtained from optimized bottom-gate, top-contact (BG-TC) transistor architecture employing spray coated Nd_2O_3 gate dielectrics and ZnO semiconducting channels both also spray coated from solutions.[55,60]

Conversion of the neodymium(III) 2,4-pentanedionate precursor into Nd_2O_3 films is achieved by spray pyrolysis above 380 ºC. Indeed, thermogravimetric analysis of neodymium(III) 2,4-pentanedionate (data not shown) revealed no further mass loss at temperatures in excess of 380 ºC. The latter was further verified by FTIR measurements (data not shown) that revealed no

features related to organic residues in the film. However, prolonged exposure of the Nd_2O_3 films in air for more than 3 days resulted in the formation of a thin layer of $Nd_2(CO_3)_3$ on the surface of the film, presumably due to atmospheric CO_2 absorption. The latter has also been reported for Nd_2O_3 films[61] deposited even from carbon-free precursors.[35] The deposition however of the ZnO semiconducting layer onto Nd_2O_3 dielectrics, prevented carbonates formation even after several weeks exposure in air, as evidenced by the absence of the carbonates features at 1370, 1470 and 1515 cm^{-1} of the FTIR spectra on KBr susbtrates (data not shown).

Figure 1a shows the Tauc[62] and Urbach[63] plots of Nd_2O_3 films on fused silica obtained by UV-Vis absorption spectroscopy. Extrapolation of the linear region of the Tauc plot to the x-axis yields the direct optical band gap of ≈6 eV comparable with that of 5.8 eV reported for epitaxial Nd_2O_3.[36,64] The Urbach tail energy of $Nd_2O_3$was found to be relatively low (about 200 meV) for solution processed dielectrics,[57,59] indicating high static order perhaps due to the formation of crystalline Nd_2O_3. Furthermore, the optical properties of Nd_2O_3 films on c-Si were investigated by *ex-situ* UV–visible spectroscopic ellipsometry in the range of photon energies between 1.5 to 4.5 eV. The data were analyzed on a basis of the Lorentz classical model, including a term for the infinite dielectric constant, as discussed in detail in the experimental section. It was found that the use of two oscillators that model contributions from low and high energy band-to-band transitions yields an excellent fit to the data as shown in Figure 1c. The modelled dispersion of the refractive index and the extinction coefficient in the photon range between 1 and 10 eV is illustrated in Figure 1b. The optical band gap of ≈6 eV, as obtained from spectroscopic ellipsometry, is in excellent agreement with that derived from UV-Vis absorption spectroscopy. Spectroscopic ellipsometry data analysis was also provided with a high-frequency dielectric constant, ε_∞ of 3.4 which in turn was used to calculate the Schottky barrier pinning factor,[65] S ≈0.63.

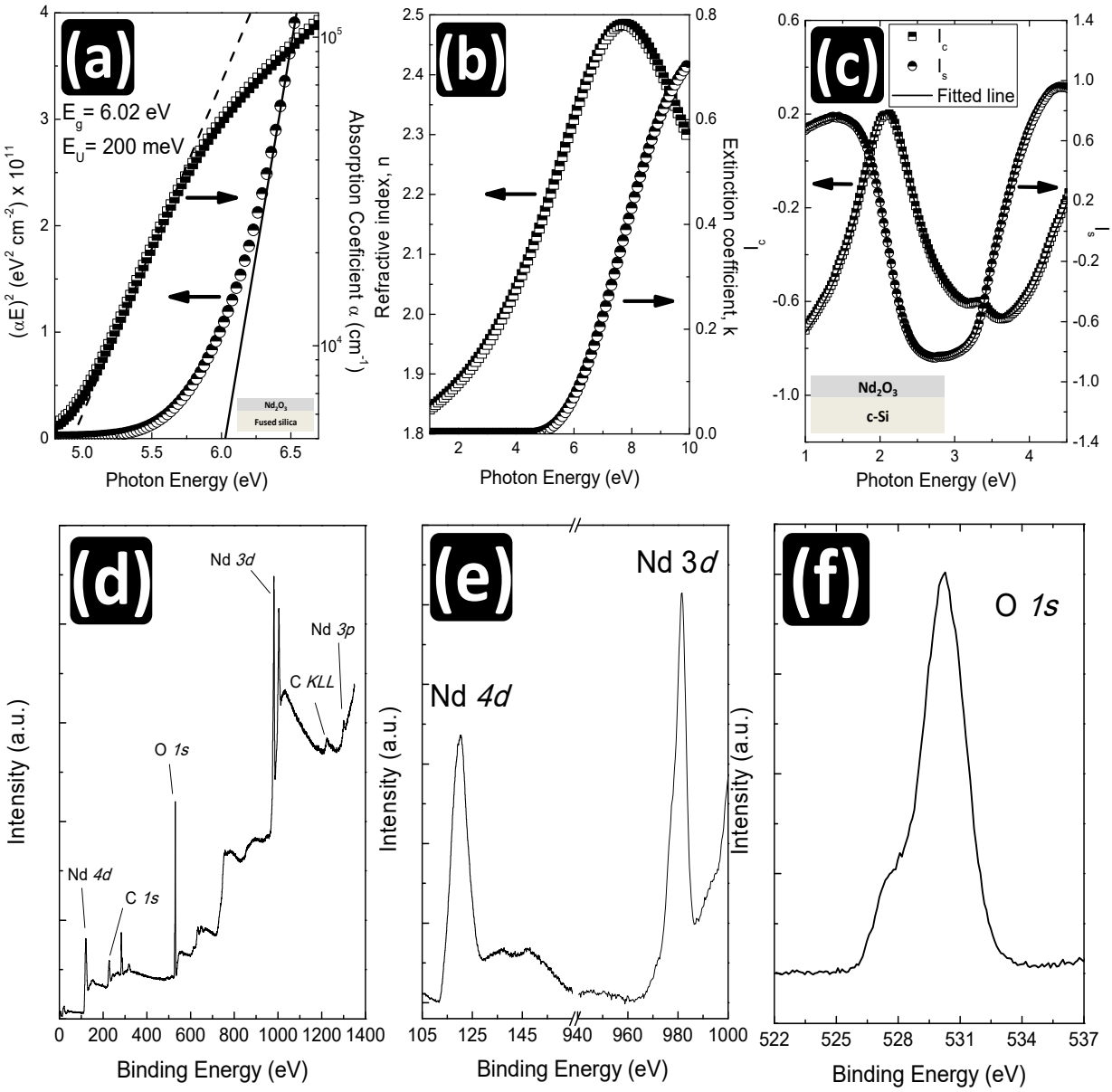

Figure 1:a) Tauc and absorption coefficient plots of Nd_2O_3 on fused silica substrate deposited at 400 ºC.**b)** Refractive index and extinction coefficient of Nd_2O_3 films spray coated at 400 ºC on c-Si as derived from spectroscopic ellipsometry. **c)** Experimental data and fitted lines of the parameters I_S=sin2ΨsinΔ and I_C= sin2ΨcosΔ of Nd_2O_3films sprayed coated at ≈400 ºC on c-Si. The fitted lines were calculated by means of a Lorentz classical model including a term of the infinite dielectric constant. **d)** Wide scan XPS spectra of Nd_2O_3films (≈60 nm) sprayed coated at ≈400 ºC on silicon substrates. **e)** Nd *4d*, Nd *3d* and **f)** O *1s* XPS spectra.

The elemental composition, binding status and stoichiometry of the Nd_2O_3 films were investigated by XPS. The XPS spectrum of solution processed Nd_2O_3 in the broad energy range between 15 eV and 1400 eV is depicted in Figure 1d. The prominent features observed were the Nd *4d*, Nd *3d* and O *1s* photoemission peaks at binding energies of ≈120 eV, ≈982 eV and

≈531 eV respectively as shown in the narrow region energy scans that are illustrated in Figure 1e and Figure 1f. The relative atomic concentration ratio Nd:O was calculated in turn from the intensities of the major photoelectron peaks by means of codes in the instrument data system employing Scofield cross sections[66] and was found to be 0.67 confirming elemental Nd_2O_3 films. As mentioned earlier however, prolonged film exposure in air, results in atmospheric CO_2 absorption so the XPS spectrum of the exposed Nd_2O_3 films also reveals C-O and O-C=O groups on the surface. Notably, no features from any other elements contributed to the spectrum. The narrow region energy scans illustrated in Figure 1e and 1f allowed determination of the chemical state of the specific elements identified. In particular, the O *1s* peak at ≈531 eV is a clear signature of oxygen in Nd_2O_3.[67] The presence of negligible carbon content (C *1s* feature at ≈284 eV) is due to the minimal exposure of this Nd_2O_3 sample to air prior to measurement. The surface morphology of spray coated Nd_2O_3 and spray coated ZnO (i.e. the semiconducting channel) onto Nd_2O_3 films on ITO-coated glass was further characterized by AFM and UFM. The images presented in **Figure 2** are the raw images after having been flattened out. The film surface was investigated in terms of root-mean-square roughness and this was found to be ≈2.7 nm for Nd_2O_3 considerably different from that of the underlying ITO (1.2 nm) that was previously reported,[68] indicating that the Nd_2O_3 films surface morphology and growth were dominated by the deposition process itself. Equally, the higher resolution UFM image in Figure 2b further demonstrates smooth and nanoporous-free films. Additionally, the uniformity in the friction images that are depicted in Figure 2c further support the fact that Nd_2O_3 films of a single phase and/or orientation were deposited. The small differences in friction at the grain boundaries are due to changes in topography, as can be concluded by comparing the AFM/UFM (normal forces) and friction (lateral forces) images.[69-71] The same findings also apply for the spray coated ZnO semiconducting layers (Figure 2d, 2e and 2f) that were sequentially deposited from solutions onto the Nd_2O_3 dielectrics.

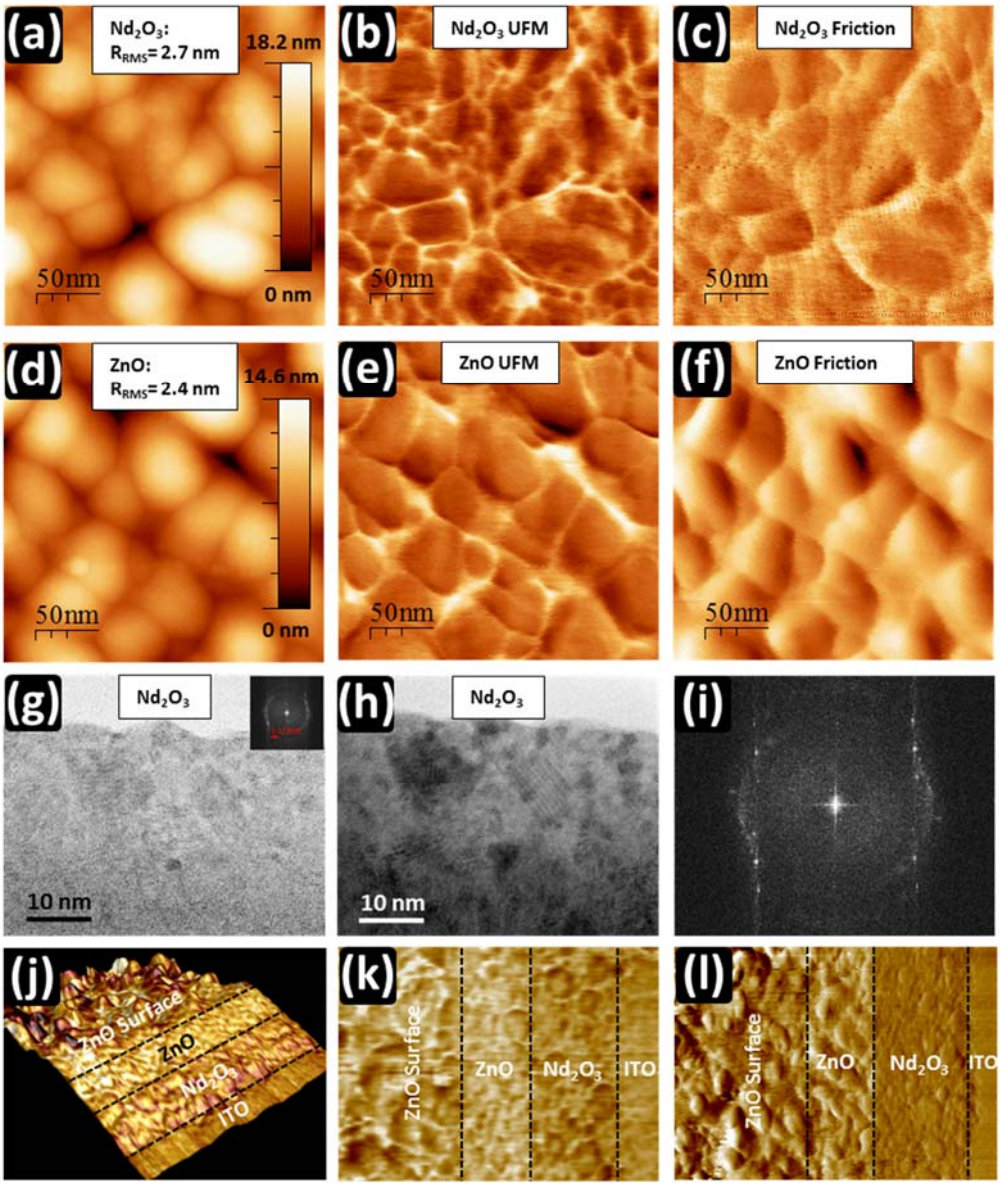

Figure 2: a) AFM topography, **b)** UFM and **c)** friction images of Nd_2O_3 films (≈36 nm) on ITO-coated glass. **d)** AFM topography, **e)** UFM and **f)** friction images of ZnO films (≈20 nm) spray coated on glass/ITO/Nd_2O_3 stacks. **g)** bright and **h)** field image of Nd_2O_3 on c-Si **i)** FFT of the high resolution image of Nd_2O_3. **j)** UFM 3D representation of the glass/ITO/Nd_2O_3 stack cross section, **k)** UFM image of the glass/ITO/Nd_2O_3 stack cross section, **l)** friction image of the glass/ITO/Nd_2O_3 stack cross section.

More insight into the nanostructure of spray coated Nd_2O_3 was obtained by Transmission Electron Microscopy. Figure 2g and 2h depict the high-resolution (HREM) and the bright field image of a 60 nm thick Nd_2O_3 film. We observe a nanostructured material, with domains of 10 nm or less in size. The structure show larger crystals nearer to the film's surface, indicating some agglomeration, consisting however of smaller sub-domains of the order of ≈10 nm. The

electron diffraction rings as shown in Figure 2 are indexed to the cubic phase Nd_2O_3 (ICSD code 96204). However, the second ring of the high resolution Fast Fourier transform image FFT (Figure 2i) is not complete in the direction parallel to the substrate. We can thus infer that particles leading to this diffraction pattern show a general vertical alignment along the (114) and (330) directions. The cross section[72] of the glass/ITO/Nd_2O_3/ZnO stack was further investigated by UFM and AFM, as illustrated in Figure 2j. The UFM and friction images that are depicted in Figure 2k and 2l further demonstrate good interface quality between the Nd_2O_3 dielectric and the ZnO semiconducting channel, as well as between the dielectric and the ITO gate electrode, revealing no foreign material phases - only those of ZnO, Nd_2O_3 and ITO.

The dielectric and leakage current properties of spray coated Nd_2O_3 dielectrics were investigated by employing a metal-insulator-metal architecture device. Nd_2O_3 films of typical thickness of ≈36 nm were sandwiched between ITO and Au top electrodes. The current density as a function of the applied electric field is illustrated in **Figure 3**a. Notably the device exhibited a high dielectric strength, with dielectric breakdown in excess of 5 MV/cm and low leakage currents as low as ≈0.5 nA/cm^2 at 1 MV/cm, a field level at which the ZnO-based TFTs operate in saturation, as will be shown later.

Similarly, the dielectric properties were further investigated by means of admittance spectroscopy. The dielectric constant dispersions in frequencies between 100 Hz and 10 MHz are shown in figure 3d. The static dielectric constant at 1 kHz, as calculated from Bode plots over a wide range of contact sizes (comparable with the area of the thin film transistors that have been subsequently manufactured using Nd_2O_3 dielectrics) and film thicknesses (in the range between 20 and 100 nm), was found to be of about 11.3. Excellent reproducibility was also found, as shown in the inset of Figure 3d. This finding is in agreement with those results obtained for cubic Nd_2O_3 that was deposited using a wide range of vacuum-based techniques.[6,41,73]

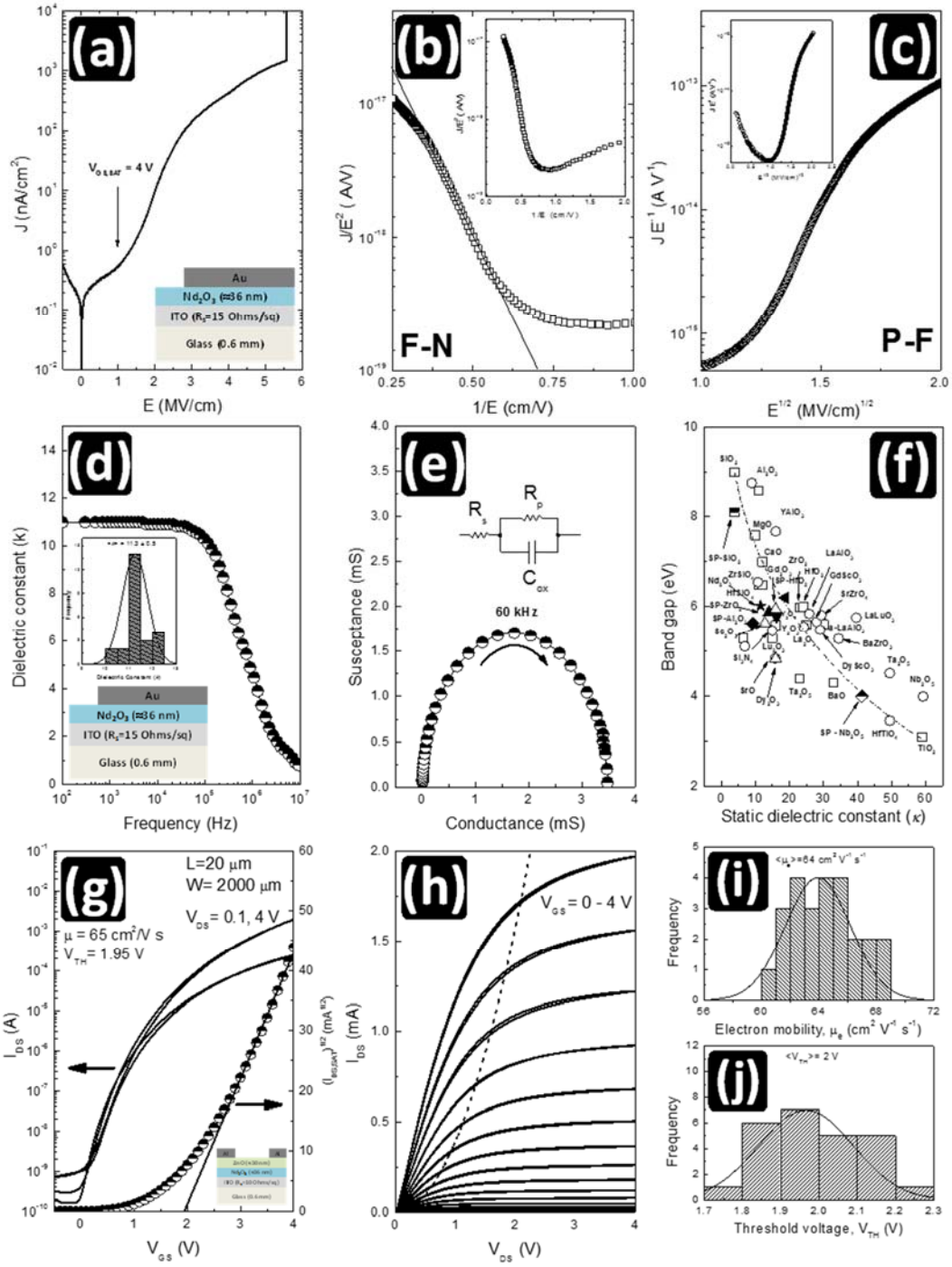

Figure 3: a) Leakage current density, **b)** Fowler-Nordheim plot (inset: full range Fowler-Nordheim plot) **c)** Poole-Frenkel plot (inset: full range Poole-Frenkel plot), **d)** dielectric constant dispersion in the frequency range between 100 Hz and 10 MHz,and **e)** Nyquist plot, of a ≈36 nm Nd_2O_3 MIM device deposited by spray pyrolysis at ≈400 ºC. **f)** Static dielectric constant versus band gap of oxide gate dielectrics grown by vacuum (empty symbols) and solution-based techniques (solid symbols). **g)** Linear (V_{DS} = 0.1 V) and saturated (V_{DS} = 4 V) transfer and **h)** output characteristics of a BGTC TFT with channel width W= 2000 μm and channel length L = 20 μm, employing solution processed ZnO semiconducting channel on a C_{ox}≈270nF/cm^2 spray coated Nd_2O_3 dielectric. **i)** Field effect mobility and **j)** threshold voltage histograms of ZnO-based TFTs employing solution processed Nd_2O_3 gate dielectrics that were manufactured under the identical conditions onto ITO-coated glass. The data obtained from TFTs with W = 2000 μm and L = 20 μm.

To further determine the conduction mechanism, Fowler Nordheim (F-N) and Poole-Frenkel (P-F) plots are shown in Figure 3b and 3c respectively. F-N plots show some linearity at high electric fields, potentially indicating an interface limited process. On the other hand, the P-F plots don't present any (or very limited) linearity, therefore a bulk limited conduction mechanism can be ruled out. Similarly, a potential space charge limited conduction (SCLC) mechanism has equally been ruled out. However, despite these indications, further work is required in order that the conduction mechanism(s) can be safely identified. To note that similar results have recently been reported for solution processed SiO_2.[68]

The Nyquist plot that is illustrated in Figure 3e, further demonstrates films of excellent dielectric properties as is also indicated by the equivalent circuit (inset of Figure 3e) that consists of a small series and large parallel resistance. Figure 3f further demonstrates the trade-off between the static dielectric constant and optical band gap of solution-processed Nd_2O_3, as well as for a number of other both solution and vacuum processed gate dielectrics.[7]

Finally, the performance of solution processed Nd_2O_3 gate dielectrics has been investigated by their implementation as gate dielectrics in bottom-gate, top-contact thin films transistors employing a ≈25 nm thick solution processed ZnO semiconducting channel[55] and aluminum source and drain contacts. The transfer and output characteristics of a typical ZnO TFT employing a ≈36 nm Nd_2O_3 gate dielectric (C_{ox} = 270 nF/cm^2) are illustrated in Figure 3g and Figure 3h respectively. Evidently, the device performance is confirmed by a high on/off current modulation ratio in the range between 10^6 and 10^7, high electron mobility $\mu_e \approx 65$ cm^2 V^{-1} s^{-1}, threshold voltage V_{TH} of ≈1.95 V and interfacial trap density on the order between 10^{11} and 10^{12} cm^{-2}, comparable with those reported for equally solution processed TFTs.[55,57,59] TFT devices employing gold source and drain contacts showed excellent stability under constant bias stress (3000 s at V_{DS} and V_{GS} =4 V, data not shown). V_{TH} increased by 12 % and field effect mobility decreased by less than 10 %.

The yield metric for spray coated TFTs, in terms of device reproducibility is demonstrated in Figure 3i and Figure 3j where the histograms of the field effect mobility and threshold voltage are illustrated. The data shown in Figure 3i and 3j were obtained from TFTs with L = 20 μm and W = 2000 μm that were deposited under identical conditions.

In summary, we have demonstrated solution processed Nd_2O_3 thin films that were deposited under ambient conditions at moderate temperatures of about 400 °C. Their implementation as gate dielectrics in thin film transistors employing solution processed ZnO semiconducting channels was also demonstrated. The optical, dielectric, electric, structural, surface and interface properties of Nd_2O_3 films were investigated using a wide range of characterization techniques that revealed smooth Nd_2O_3 films of cubic structure, wide band gap (≈6 eV), high-*k* (≈11 - 12), and low leakage currents (<0.5 nA/cm^2 at 1 MV/cm). Moreover, TFTs using ZnO as the channel material showed excellent characteristics, such as high electron mobility, in excess of 65 cm^2 V^{-1}s^{-1}, high on/off current ratio in the range 10^6 and 10^7 and negligible hysteresis. The devices (employing gold source and drain contacts) demonstrated excellent constant bias stress and air stability air i.e. only a small decrease of the electron mobility and threshold voltage (< 12%). In addition, the excellent uniformity and homogeneity that was demonstrated combined with the relatively low deposition temperature (compared with those used with the vast majority of the vacuum based techniques employed elsewhere) in ambient air on glass substrates indicates the potential for the rapid development of metal oxide-based TFTs employing gate dielectrics also grown from solutions at low manufacturing cost.

Experimental Section

Nd_2O_3 Deposition by Spray Pyrolysis: A 30 mg/ml precursor solution of Neodymium(III) 2,4-pentanedionate was prepared in methanol, pentane-2,4-dione, N,N-Dimethyloformamide (7:2:1) and the solution was stirred at room temperature for about 5 hours. The substrates were kept at 400ºC on a hotplate, while aerosols of the solution were sprayed onto the glass substrates

employing a pneumatic airbrush, held at a vertical distance of about 30 cm above the substrate. After a period of 10 s, the spray process was interrupted for 60 s to allow for the vapors to settle onto the substrates before the cycle was repeated until films of typical thicknesses in the range between 20 and 80 nm were obtained. This process yielded films of excellent homogeneity (thickness standard deviation < 3%) over an area of 18 cm x 18 cm.

ZnO: The ZnO semiconducting channels were spray coated on glass/ITO/Nd_2O_3 (≈36 nm) stacks (kept at 400 °C) from 25 mg/mL zinc acetate ($Zn(CH_3CO_2)_2$) solutions in methanol until films of typical thickness of ≈20 nm were obtained.

Atomic force microscopy (AFM), ultrasonic force microscopy (UFM): Contact mode AFM was used to study the topography of the spray coated Nd_2O_3 and ZnO. The measurements were performed in ambient conditions using a Bruker Nanoscope III system and standard contact mode cantilevers (Contact-G, Budget Sensors, k = 0.2 N m^{-1}). Also UFM measurements were carried out in ambient conditions using a modified version of the above system and performed using a 4 MHz carrier frequency and 2.7 kHz modulation frequency using samples mounted on a 4 MHz thickness resonance piezoplate (PI) calibrated via a laser Doppler vibrometer (Polytec OFV-534). To note that the surface damage to the sample and the tip during UFM imaging is negligible because of the effect of ultrasound-induced lubricity that eliminates the shear forces during the scanning.[74]

Beam-Exit Cross-Sectional Polishing: The glass/ITO/Nd_2O_3 stacks were mounted on a BEXP angled holder (5° slope) with an overhang of ≈300 μm. The beam entry surface was then filed down normal to the beam direction with 30, 9, and then 1 μm diamond paper. The holder was placed within the vacuum chamber and BEXP was initiated at a vacuum of 2.0×10^{-5} mbar. Ion guns were allowed to warm up at a voltage of 3 kV for 10 min prior to processing at 6 kV. Once beam-exit occurred, voltage was decreased to 1 kV for 20 min to polish the surface. The process resulted in a cut of approximately 11° through the area of interest (with respect to the

sample surface). Samples were subsequently cleaned in an ultrasonic bath using trichloroethylene, acetone and isopropanol for 10 minutes each.

X-ray Photoelectron Spectroscopy (XPS): XPS measurements of Nd_2O_3 on ITO were conducted using a Thermofisher ESCALAB 250 electron spectrometer equipped with a hemispherical sector energy analyzer. An Al K_α x-ray source was used for analysis at source excitation energy of 15 keV and emission current of 6 mA. An analyzer pass energy of 20 eV with step size of 0.1 eV and dwell time of 50 ms was used throughout the experiments. The base pressure within the spectrometer during examinations was always lower than 5 x 10^{-10} mbar and this ensured that all signals recorded were from the sample surface and no contamination was introduced from the vacuum chamber.

Transmission Electron Microscopy: Nd_2O_3 films of typical thickness of ≈60 nm were characterized by high resolution transmission electron microscopy using a Hitachi HD-2300A Hitachi HD-2300A scanning transmission electron microscope (200 keV acceleration voltage, Schottky field emission source). The films were mechanically ground and polished, followed by precision ion beam polishing (Gatan PIPS^{TM}) at 4.5keV, 4.5°, to create an electron-beam transparent region.

UV–Vis Absorption Spectroscopy: Optical transmission spectra of Nd_2O_3 on fused silica were measured at wavelengths between 180 nm and 1000 nm using an Agilent Cary 5000 spectrometer.

Spectroscopic Ellipsometry: SE and Variable Angle Spectroscopic Ellipsometry (VASE) measurements of Nd_2O_3 films on intrinsic c-Si were performed in ambient conditions at incidence angles between 60º and75° using a Jobin–Yvon UVISEL phase modulated system over the spectral range 1 eV to 4.5 eV. The data were analyzed in terms of the Lorentz classical model that takes into account interband transitions where the electron moves to a final state in a different band without changing its k-vector in the Brillouin's zone. For N Lorenz oscillators

the complex dielectric function is assumed to be equal to the sum of contributions from individual oscillators as follows:

$$\varepsilon(\omega) = \varepsilon_{\infty} + \sum_{j=1}^{N} \frac{f_j \cdot \omega_{oj}^2}{\omega_{oj}^2 - \omega^2 + +i \cdot \gamma_j \cdot \omega}$$

where ε_{∞} is the high frequency dielectric constants, f_j is the oscillator strength, ω_{oj} the resonant energy of an oscillator and γ_j the broadening parameter corresponding to the peak energy of each oscillator. Modelling the SE data on c-Si assumed a homogenous Nd_2O_3 layer. However, a thin layer (<4 nm) of SiO_2 between the c-Si substrate and Nd_2O_3 layer was also accounted for and further confirmed by TEM. The assumption of two Nd_2O_3 layers (i.e. a thin top Nd_2O_3 to model the roughness) didn't affected the fitting's quality or the dielectric function dispersion.

Impedance spectroscopy: Impedance spectroscopy measurements on Metal Insulator Metal (MIM) devices (glass/ITO/Nd_2O_3/Au) were performed using a Solartron 1260 impedance/gain-phase analyzer at frequencies between 100 Hz and 10 MHz applying a 50 mV AC voltage. The Au electrodes were thermally evaporated on glass/ITO/Nd_2O_3 stacks under high vacuum (10^{-7} mbar) through a shadow mask.

TFTs Fabrication/Characterization: Bottom Gate – Top Contact (BG–TC) transistors were fabricated. Aluminum (Al) source and drain (S/D) electrodes (50 nm) were thermally evaporated under high vacuum (10^{-7} mbar) through a shadow mask onto the glass/ITO/Nd_2O_3/ZnO stacks. Device characterization was carried out under high vacuum (10^{-5} mbar), at room temperature using an Agilent B1500A semiconductor parameter analyzer. Electron mobility and interfacial trap density were extracted from the transfer curves in both the linear and saturation regime using the gradual channel approximation.

$$\mu_{e,lin} = \frac{L}{C_i W V_D} \frac{\partial I_{DS}}{\partial V_{GS}}$$

$$\mu_{e,sat} = \frac{L}{C_i W} \frac{\partial^2 I_{DS}}{\partial^2 V_{GS}}$$

$$D_{it} = \left[\frac{SS \times 0.4334}{kT/q} - 1\right]\frac{C_i}{q}$$

where SS is the subthreshold swing and kT/q the thermal voltage (at 300 K).

Acknowledgements

M.E. is grateful for support from the Ministry of Education Malaysia and Faculty of electronics and Computer Engineering, Universiti Teknikal Malaysia Melaka (UteM).

Received: ((will be filled in by the editorial staff))
Revised: ((will be filled in by the editorial staff))
Published online: ((will be filled in by the editorial staff))

References

[1] J. Robertson, *J. Vac. Sci. Technol. B* **2000**, *18*, 1785.
[2] G. D. Wilk, R. M. Wallace, J. M. Anthony, *J. Appl. Phys.* **2001**, *89*, 5243.
[3] J. Robertson, *Reports Prog. Phys.* **2006**, *69*, 327.
[4] M. Leskelä, M. Ritala, *J. Solid State Chem.* **2003**, *171*, 170.
[5] A. C. Jones, H. C. Aspinall, P. R. Chalker, R. J. Potter, K. Kukli, A. Rahtu, M. Ritala, M. Leskela, *J. Mater. Chem.* **2004**, *14*, 3101.
[6] J. Päiväsaari, M. Putkonen, L. Niinistö, *Thin Solid Films* **2005**, *472*, 275.
[7] J. Robertson, R. M. Wallace, *Mater. Sci. Eng. R Reports* **2015**, *88*, 1.
[8] H. Ono, T. Katsumata, *Appl. Phys. Lett.* **2001**, *78*, 1832.
[9] K. J. Hubbard; D. G. Schlom, *J. Mater. Res.* **1996**, *11*, 2757.
[10] M. Hong, *Science (80-.).* **1999**, *283*, 1897.
[11] M. Passlack, R. Droopad, Z. Yu, N. Medendorp, D. Braddock, X. W. Wang, T. P. Ma, T. Büyüklimanli, *IEEE Electron Device Lett.* **2008**, *29*, 1181.
[12] J. Robertson, L. Lin, *Microelectron. Eng.* **2011**, *88*, 1440.
[13] L. Lin, J. Robertson, *Appl. Phys. Lett.* **2011**, *98*, 8.
[14] X. Yu, T. J. Marks, A. Facchetti, *Nat. Mater.* **2016**, *15*, 383.
[15] S. R. Thomas, P. Pattanasattayavong, T. D. Anthopoulos, *Chem. Soc. Rev.* **2013**, *42*, 6910.
[16] T. Kamiya, K. Nomura, H. Hosono, *Sci. Technol. Adv. Mater.* **2010**, *11*, 44305.
[17] E. Fortunato, P. Barquinha, R. Martins, *Adv. Mater.* **2012**, *24*, 2945.
[18] H. Yabuta, M. Sano, K. Abe, T. Aiba, T. Den, H. Kumomi, K. Nomura, T. Kamiya, H. Hosono, *Appl. Phys. Lett.* **2006**, *89*, 112123.
[19] K. Nomura, H. Ohta, A. Takagi, T. Kamiya, M. Hirano, H. Hosono, *Nature* **2004**, *432*, 488.
[20] Y.-H. Lin, S. R. Thomas, H. Faber, R. Li, M. A. McLachlan, P. A. Patsalas, T. D. Anthopoulos, *Adv. Electron. Mater.* **2016**, *2*, 1600070.
[21] S. P. Chang, S. S. Shih, *J. Nanomater.* **2012**, *2012*, 10.
[22] J. S. Park, T. S. Kim, K. S. Son, J. S. Jung, K. Lee, J. Kwon, B. Koo, S. Lee, *Nano* **2010**, *31*, 440.

[23] P. Barquinha, A. M. Vila, G. Gonçalves, L. Pereira, R. Martins, J. R. Morante, E. Fortunato, *IEEE Trans. Electron Devices* **2008**, *55*, 954.
[24] J. Robertson, C. W. Chen, *Appl. Phys. Lett.* **1999**, *74*, 1168.
[25] D. Saikia, P. K. Saikia, *ECS Solid State Lett.* **2015**, *4*, Q51.
[26] T. Busani, R. Devine, P. Gonon, in *ECS Trans.*, ECS, **2006**, pp. 331–340.
[27] T. Gerfin, M. Becht, K.-H. Dahmen, *Berichte der Bunsengesellschaft für Phys. Chemie* **1991**, *95*, 1564.
[28] V. D. Kushkov, A. M. Zaslavskii, A. V Zverlin, A. V Melnikov, *J. Mater. Sci. Lett.* **1991**, *10*, 1111.
[29] T.-M. Pan, J.-D. Lee, W.-H. Shu, T.-T. Chen, *Appl. Phys. Lett.* **2006**, *89*, 232908.
[30] M. H. Masaaki Imura, Terumi Tanaka, and M. Okada, *Mater. Trans. JIM* **1994**, *35*, 730.
[31] X. D. Wu, L. Luo, S. R. Foltyn, R. C. Dye, N. S. Nogar, L. Alamos, **1992**, *21*, 495.
[32] S. J. S. Jeon, K. I. K. Im, H. Y. H. Yang, H. L. H. Lee, H. S. H. Sim, S. C. S. Choi, T. J. T. Jang, H. H. H. Hwang, *Int. Electron Devices Meet. Tech. Dig. (Cat. No.01CH37224)* **2001**, 9.
[33] M. D. Kannan, S. K. Narayandass, C. Balasubramanian, D. Mangalaraj, *Phys. status solidi* **1991**, *128*, 427.
[34] M. D. Kannan, S. K. Narayandass, C. Balasubramanian, D. Mangalaraj, *Phys. status solidi* **1990**, *121*, 515.
[35] G. D. Dhamale, V. L. Mathe, S. V Bhoraskar, S. N. Sahasrabudhe, S. D. Dhole, S. Ghorui, *Nanotechnology* **2016**, *27*, 85603.
[36] A. Fissel, Z. Elassar, O. Kirfel, E. Bugiel, M. Czernohorsky, H. J. Osten, *J. Appl. Phys.* **2006**, *99*, DOI 10.1063/1.2188051.
[37] S. Seppälä, J. Niinistö, T. Blanquart, M. Kaipio, K. Mizohata, J. Räisänen, C. Lansalot-Matras, W. Noh, M. Ritala, M. Leskelä, *Chem. Mater.* **2016**, *28*, 5440.
[38] P.-A. Hansen, H. Fjellvåg, T. Finstad, O. Nilsen, *Dalt. Trans.* **2013**, *42*, 10778.
[39] J. Päiväsaari, M. Putkonen, L. Niinistö, *Thin Solid Films* **2005**, *472*, 275.
[40] H. Ono, T. Katsumata, *Appl. Phys. Lett.* **2001**, *78*, 1832.
[41] A. Kosola, J. Päiväsaari, M. Putkonen, L. Niinistö, *Thin Solid Films* **2005**, *479*, 152.
[42] X. Fan, H. Liu, C. Fei, *Mater. Res. Express* **2014**, *1*, 45005.
[43] X. Fan, H. Liu, C. Fei, B. Zhong, X. Wang, Q. Wang, *J. Electron. Mater.* **2015**, *44*, 2592.
[44] G. Bonnet, M. Lachkar, J. C. Colson, J. P. Larpin, *Thin Solid Films* **1995**, *261*, 31.
[45] S. Chevalier, G. Bonnet, J. P. Larpin, *Appl. Surf. Sci.* **2000**, *167*, 125.
[46] Y. Tasaki, M. Satoh, S. Yoshizawa, H. Kataoka, H. Hidaka, *Japanese J. Appl. Physics, Part 1 Regul. Pap. Short Notes Rev. Pap.* **1997**, *36*, 6871.
[47] P. Taechakumput, C. Z. Zhao, S. Taylor, M. Werner, P. R. Chalker, J. M. Gaskell, H. C. Aspinall, A. C. Jones, S. Chen, *J. Nanomater.* **2012**, *2012*, 1.
[48] Y. F. Loo, R. J. Potter, A. C. Jones, H. C. Aspinall, J. M. Gaskell, P. R. Chalker, L. M. Smith, G. W. Critchlow, *Chem. Vap. Depos.* **2004**, *10*, 306.
[49] T. Sreethawong, S. Chavadej, S. Ngamsinlapasathian, S. Yoshikawa, *Solid State Sci.* **2008**, *10*, 20.
[50] C. Wang, X. Shao, Q. Su, Z. Cheng, G. Zhao, *Phys. status solidi* **1997**, *162*, 623.
[51] R. Yuvakkumar, S. I. Hong, *J. Sol-Gel Sci. Technol.* **2015**, *73*, 511.
[52] M. Langlet, R. D. Shannon, *Thin Solid Films* **1990**, *186*, L1.
[53] T. Katsumata, T. Murakami, Y. Happo, S. Komuro, *J. Cryst. Growth* **1999**, *198–199*, 1226.
[54] M. Zawadzki, L. Kępiński, *J. Alloys Compd.* **2004**, *380*, 255.
[55] M. Esro, G. Vourlias, C. Somerton, W. I. Milne, G. Adamopoulos, *Adv. Funct. Mater.* **2015**, *25*, 134.

[56] G. Adamopoulos, S. Thomas, P. H. Wöbkenberg, D. D. C. Bradley, M. A. McLachlan, T. D. Anthopoulos, *Adv. Mater.* **2011**, *23*, 1894.
[57] D. Afouxenidis, R. Mazzocco, G. Vourlias, P. J. Livesley, A. Krier, W. I. Milne, O. Kolosov, G. Adamopoulos, *ACS Appl. Mater. Interfaces* **2015**, *7*, 7334.
[58] G. Adamopoulos, S. Thomas, D. D. C. Bradley, M. a. McLachlan, T. D. Anthopoulos, **2011**, *123503*, 98.
[59] M. Esro, R. Mazzocco, G. Vourlias, O. Kolosov, a. Krier, W. I. Milne, G. Adamopoulos, *Appl. Phys. Lett.* **2015**, *106*, 203507.
[60] G. Adamopoulos, A. Bashir, W. P. Gillin, S. Georgakopoulos, M. Shkunov, M. a. Baklar, N. Stingelin, D. D. C. Bradley, T. D. Anthopoulos, *Adv. Funct. Mater.* **2011**, *21*, 525.
[61] S. Bernal, F. J. Botana, R. García, J. M. Rodríguez-Izquierdo, *J. Mater. Sci.* **1988**, *23*, 1474.
[62] J. Tauc, R. Grigorovici, A. Vancu, *Phys. status solidi* **1966**, *15*, 627.
[63] F. Urbach, *Phys. Rev.* **1953**, *92*, 1324.
[64] A. Laha, A. Fissel, E. Bugiel, H. J. Osten, *Thin Solid Films* **2007**, *515*, 6512.
[65] W. Mönch, *Phys. Rev. Lett.* **1987**, *58*, 1260.
[66] E. B. Saloman, J. H. Hubbell, J. H. Scofield, *At. Data Nucl. Data Tables* **1988**, *38*, 1.
[67] T.-M. Pan, J.-D. Lee, W.-W. Yeh, *J. Appl. Phys.* **2007**, *101*, 24110.
[68] M. Esro, O. V. Kolosov, P. J. Jones, W. I. Milne, G. Adamopoulos, *ACS Appl. Mater. Interfaces* **2016**, acsami.6b11214.
[69] R. M. Overney, E. Meyer, J. Frommer, D. Brodbeck, R. Lüthi, L. Howald, H.-J. Giintherodt, M. Fujihira, H. Takano, Y. Gotoh, *Nature* **1992**, *359*, 133.
[70] D. Gourdon, N. A. Burnham, A. Kulik, E. Dupas, D. Stamou, M. Liley, H. Vogel, C. Duschl, F. Oulevey, G. Gremaud, Z. Dienes, others, *Trib. Lett.* **1997**, *3*, 317.
[71] S. Grafstrom, M. Neitzert, T. Hagen, J. Ackermann, R. Neumann, O. Probst, M. Wortge, *Nanotechnology* **1993**, *4*, 143.
[72] A. J. Robson, I. Grishin, R. J. Young, A. M. Sanchez, O. V Kolosov, M. Hayne, *ACS Appl. Mater. Interfaces* **2013**, *5*, 3241.
[73] M.-K. Song, S.-W. Rhee, *Thin Solid Films* **2005**, *492*, 19.
[74] F. Dinelli, S. K. Biswas, G. A. D. Briggs, O. V Kolosov, *Appl. Phys. Lett.* **1997**, *71*.

TOC graphic

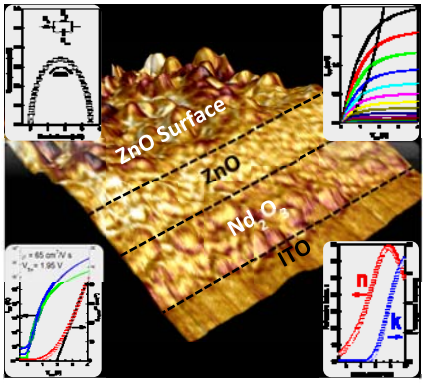

Solution-processed metal oxide thin film transistors (TFTs) employing spray coated Neodymium Oxide (Nd_2O_3) gate dielectrics and spray coated zinc oxide (ZnO) semiconducting channels are demonstrated. The TFTs show excellent characteristics in terms of negligible hysteresis, low operation voltage and leakage currents, high on/off current modulation of about 10^6 and electron mobility exceeding 65 $cm^2\ V^{-1}\ s^{-1}$.